Imaging the Enzyme 11β-Hydroxysteroid Dehydrogenase Type 1 with PET: Evaluation of the Novel Radiotracer ^{11}C-AS2471907 in Human Brain

Jean-Dominique Gallezot[1], Nabeel Nabulsi[1], Shannan Henry[1], Richard Pracitto[1], Beata Planeta[1], Jim Ropchan[1], Shu-Fei Lin[1], David Labaree[1], Michael Kapinos[1], Anupama Shirali[1], Teresa Lara-Jaime[1], Hong Gao[1], David Matuskey[1], Mark Walzer[2], Gerard J. Marek[2], Susan Bellaire[3], Nancy Yuan[4], Richard E. Carson[1], and Yiyun Huang[1]

[1]Department of Radiology and Biomedical Imaging, Yale University School of Medicine, New Haven, Connecticut; [2]Astellas Pharma Global Development, Northbrook, Illinois; [3]Astellas Pharma Europe BV, Leiden, The Netherlands; and [4]Astellas Pharma Global Development, Northbrook, Illinois

The 11β-hydroxysteroid dehydrogenase type 1 (11β-HSD1) enzyme converts cortisone to cortisol and participates in the regulation of glucocorticoid levels in tissues. 11β-HSD1 is expressed in the liver, kidney, adipose tissue, placenta, and brain. 11β-HSD1 is a target for treatment of depression, anxiety, posttraumatic stress disorder, and also against age-related cognitive function and memory loss. In this study, we evaluated the radiotracer ^{11}C-AS2471907 (3-(2-chlorophenyl)-4-(methyl-^{11}*C*)-5-[2-[2,4,6-trifluorophenoxy]propan-2-yl]-4*H*-1,2,4-triazole) to image 11β-HSD1 availability in the human brain with PET. **Methods:** Fifteen subjects were included in the study. All subjects underwent one 2-h scan after a bolus administration of ^{11}C-AS2471907. Two subjects underwent an additional scan after blockade with the selective and high-affinity 11β-HSD1 inhibitor ASP3662 to evaluate ^{11}C-AS2471907 nondisplaceable distribution volume. Five subjects also underwent an additional scan to evaluate the within-day test–retest variability of ^{11}C-AS2471907 volumes of distribution (V_T). **Results:** ^{11}C-AS2471907 time–activity curves were best fitted by the 2-tissue-compartment (2TC) model. ^{11}C-AS2471907 exhibited a regionally varying pattern of uptake throughout the brain. The V_T of ^{11}C-AS2471907 ranged from 3.7 ± 1.5 mL/cm^3 in the caudate nucleus to 14.5 ± 5.3 mL/cm^3 in the occipital cortex, with intermediate values in the amygdala, white matter, cingulum, insula, frontal cortex, putamen, temporal and parietal cortices, cerebellum, and thalamus (from lowest to highest V_T). From the blocking scans, nondisplaceable distribution volume was determined to be 0.16 ± 0.04 mL/cm^3 for ^{11}C-AS2471907. Thus, nearly all uptake was specific and the binding potential ranged from 22 in the caudate to 90 in the occipital cortex. Test–retest variability of 2TC V_T values was less than 10% in most large cortical regions (14% in parietal cortex) and ranged from 14% (cerebellum) to 51% (amygdala) in other regions. The intraclass correlation coefficient of 2TC V_T values ranged from 0.55 in the white matter to 0.98 in the cerebellum. **Conclusion:** ^{11}C-AS2471907 has a high fraction of specific binding in vivo in humans and reasonable within-day reproducibility of binding parameters.

Key Words: 11β-hydroxysteroid dehydrogenase-1; cortisol; brain; positron emission tomography

J Nucl Med 2019; 60:1140–1146
DOI: 10.2967/jnumed.118.219766

The hypothalamus, pituitary gland, and adrenal gland collectively form a complex circuit of direct influences and feedback interactions called the HPA axis. This is a major part of the neuroendocrine system and controls the response to stress and modulates a variety of processes, including digestion, mood, emotion, immune reaction, sexuality, and energy storage and consumption. Stress induces the activation of the HPA axis and release of glucocorticoids. Two enzymes are involved in the regulation of glucocorticoids and activation of glucocorticoid receptors: 11β-hydroxysteroid dehydrogenase-1 (11β-HSD1), a reductase in vivo that converts cortisone to cortisol and amplifies glucocorticoid action in a tissue-specific manner, and 11β-hydroxysteroid dehydrogenase-2 (11β-HSD2) that catalyzes the conversion of cortisol back to cortisone. 11β-HSD1 is expressed in the liver, kidney, adipose tissue, placenta, and brain, whereas 11β-HSD2 is primarily expressed in the kidney and functions mainly as a source of cortisone production. Together, glucocorticoid homeostasis is maintained by the HPA axis and activities of the 11β-HSD enzymes.

In the rodent brain, 11β-HSD1 activity is highest in the cerebellum, hippocampus, and neocortex, with levels about 10%–30% of those in kidney and liver (*1–3*). Activity in other regions of the brain are also detected, including the anterior pituitary, hypothalamus, amygdala, and brain stem (*1,3,4*). A similar expression pattern is found in the postmortem human brain (*5*). In general, the pattern of 11β-HSD1 messenger RNA expression in the brain is paralleled by those of immunohistochemistry and enzyme activity. Since 11β-HSD1 is expressed in key brain regions in the negative feedback action of glucocorticoids, this enzyme is a critical regulator of the HPA axis (*6*), and thus important in the pathophysiology of stress-related disorders such as depression, posttraumatic stress disorder, and addictive behaviors, where dysregulation of the HPA axis and glucocorticoids has been abundantly demonstrated (*7–9*). In addition to these disorders, accumulating evidence has pointed to the association of age-related cognitive

Received Feb. 10, 2018; revision accepted Jan. 7, 2019.
For correspondence or reprints contact: Jean-Dominique Gallezot, Yale University PET Center, 801 Howard Ave., P.O. Box 208048, New Haven, CT 06520-8048.
E-mail: jean-dominique.gallezot@yale.edu
Published online Mar. 15, 2019.

impairment, elevated glucocorticoid levels, and increased 11β-HSD1 expression in the brain (*10–12*). Inhibition of 11β-HSD1 has been shown to improve memory (*13*) and to protect against the decline of cognitive function with age (*5,14–16*), or the even more catastrophic memory loss associated with Alzheimer disease (AD) (*17*). Importantly, recent evidence appears to also indicate a link between insulin resistance and AD (*18*). As a result, 11β-HSD1 inhibitors, originally targeted for type 2 diabetes, have been proposed as a target for drug development to treat cognitive impairment.

PET is a powerful imaging technology for the in vivo investigation of biologic targets. The availability of PET imaging agents for 11β-HSD1 will provide noninvasive biomarkers to interrogate the enzyme in vivo in human subjects and gain insights into its function and dysfunction in diseases. Further, PET imaging with 11β-HSD1 radiotracers can be used to assess target engagement and correlate target occupancy, dose exposure, and therapeutic response of 11β-HSD1 inhibitors currently in clinical trials, thus aiding the development of novel therapeutic agents. Merck was the first to disclose a PET radiotracer for imaging 11β-HSD1 in the brain, and ligand ^{11}C-**1** (Fig. 1) was reported in a conference abstract as having good brain uptake in rhesus monkeys and specific binding in vivo that could be blocked by MK-0916, a selective 11β-HSD1 inhibitor (*19*). However, imaging studies in humans with this radiotracer have not been reported. We have previously reported ^{11}C-AS2471907 (**2**) (Fig. 1)—with a binding affinity of 2.2 nM for 11β-HSD1, greater than 10 μM for 11β-HSD2, and a minimal binding affinity for a wide range of protein targets—as a suitable PET radiotracer to image the 11β-HSD1 in the monkey brain. Here, we report the first PET imaging evaluation of ^{11}C-AS2471907 in humans to assess its pharmacokinetic characteristics, select the optimal method for quantitative analysis, examine the test–retest reproducibility of kinetic and in vivo binding parameters, and define the levels of specific binding via blocking studies.

MATERIALS AND METHODS

Study Plan and Population

The study was conducted in compliance with the ethical principles originating in or derived from the Declaration of Helsinki and in compliance with all International Conference on Harmonization Good Clinical Practice guidelines. In addition, all local regulatory requirements were followed, in particular, those affording greater protection to the safety of trial participants. These studies were performed under protocols approved by the Yale School of Medicine Human Investigation Committee, the Yale-New Haven Hospital Radiation Safety Committee, and the Yale University Radiation Safety Committee. Subjects were recruited by public advertisement. Written informed consent was obtained from all participants after full explanation of study procedures. Dosing of ASP3662 was conducted under the Astellas investigational new drug (IND 116,896).

All subjects were healthy males and had a comprehensive screening assessment that included a clinical interview, complete physical examination with medical history, routine blood tests, electrocardiogram, and urine toxicology. Individuals were excluded if they self-reported or evaluation revealed a diagnosis of a current or lifetime psychiatric disorder; a history of suicide attempts, current or past serious medical or neurologic illness (including a history of head injury with loss of consciousness); a history of substance abuse or dependence; nicotine use in the past 6 mo; prescription or nonprescription medication in the last 2 wk; or clinically significant laboratory or electrocardiogram results.

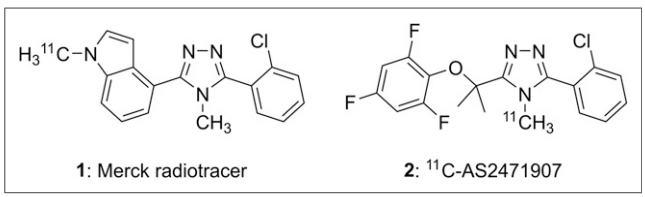

FIGURE 1. Chemical structures of radiotracers for 11β-HSD1.

Fifteen subjects were included in the study (age, 38 ± 8 y [range, 28–51 y]; body weight, 84 ± 9.7 kg [range, 69–100 kg]). Two subjects underwent an additional scan after preblockade of 11β-HSD1 by ASP3662 (*20*) (30 mg, 26 ± 3 h before tracer injection), and 5 subjects underwent a second (retest) scan on the same day to assess test–retest variability (TRV). Test scans occurred between 10 AM and 3 PM, and retest scans occurred 2.7–6.4 h later.

Radiochemistry

The reference standard AS2471907 and its *N*-desmethyl triazole precursor AS319448 were provided by Astellas Pharma Inc., Japan. ^{11}CO2 was produced with the PETTrace cyclotron (GE Healthcare) through the ^{14}N(p,α)^{11}C nuclear reaction by bombarding a high-pressure nitrogen target containing 1% oxygen with a 16.8-MeV proton beam.

The radiotracer ^{11}C-AS2471907 was prepared by *N*-^{11}C-methylation of the precursor AS319448-00 (10 mg) with ^{11}C-methyl triflate in anhydrous acetonitrile (0.2 mL) at 70°C for 5 min (Fig. 2) using the TRACERlab FXC Pro automated synthesis module (GE Healthcare). The crude reaction mixture was purified by high-performance liquid chromatography (HPLC) (YMC-pack Pro C18 column, 5 μm, 250 × 10 mm; YMC America Inc.). The column was eluted with a solvent mixture of 45% acetonitrile, 5% tetrahydrofuran, and 50% 0.04 M HCl (v/v, pH 1.4) at a flow rate of 4 mL/min and monitored by ultraviolet and radioactivity detectors. The desired radioactive product was collected, diluted with 50 mL of deionized water, and passed through a Waters C18 SepPak cartridge. The cartridge was rinsed with 10 mL of 0.001N HCl. The radioactive product was eluted off the SepPak with 1 mL of absolute ethanol (United States Pharmacopeia [USP]) followed by 3 mL of saline (USP) and collected into the FXC Pro product vial. Finally, the combined product solution was passed through a sterile 0.22-μm membrane filter for terminal sterilization and collected into a pyrogen-free collection vial precharged with 7 mL of saline (USP) and 40 μL of 4.2% sodium bicarbonate solution (USP) to afford a formulated solution ready for dispensing and administration.

Radiochemical purity and molar activity were determined by HPLC analysis of the final product solution (column: Phenomenex Luna C18(2), 5 μm, 4.6 × 250 mm; mobile phase: 52% of acetonitrile and 48% of 0.1 M aqueous ammonium formate solution containing 0.5% acetic acid, pH 4.2; flow rate: 2 mL/min; ultraviolet detector wavelength: 230 nm).

PET Data Acquisition

PET scans were obtained on the HRRT scanner (resolution, 2.5–3 mm full width at half maximum) for 120 min. During the scans, subjects wore an optical tracking tool to record head motion with an infrared detector (Vicra; NDI Systems). PET data were reconstructed with all corrections including motion (as recorded by the Vicra) using the ordered-subset expectation maximization algorithm (2 iterations, 30 subsets).To correct any residual motion due to possible slippage of the tracking tool on the subject's head, a second step of motion correction was applied to the dynamic images, using a mutual-information algorithm (FSL-FLIRT, version 3.2, Analysis Group, FMRIB) with frame-by-frame registration to a summed image (0–10 min).

Arterial Blood Measurements

Arterial blood samples were drawn from a catheter inserted in the radial artery to measure the whole blood and plasma radioactivity

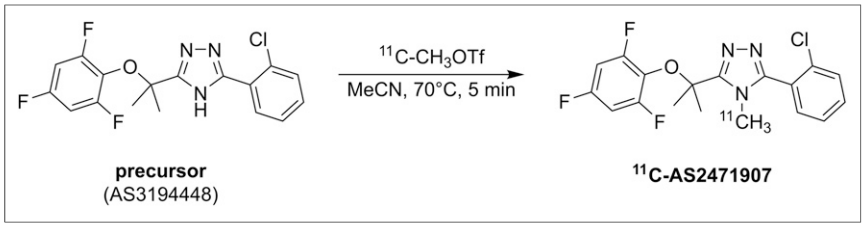

FIGURE 2. Radiosynthesis of ^{11}C-AS2471907.

curves, the metabolite-corrected plasma curve, and the plasma-free fraction as previously described (*21,22*), with modifications for the HPLC methods. In brief, plasma analysis of the radiotracer metabolism was performed from samples collected at 3, 8, 15, 30, 60, and 90 min. The automatic column-switching HPLC system was equipped with a capture column (19 × 4.6 mm) packed with Phenomenex SPE Strata-X sorbent and a Phenomenex Luna phenyl-hexyl analytic column (5 μm, 250 × 4.6 mm) with a mobile phase composed of 55% of acetonitrile and 45% of 50 mM ammonium acetate (v/v) at a flow rate of 1.55 mL/min. The retention time for ^{11}C-AS2471907 was approximately 11 min.

Computation of Time–Activity Curves

Each subject underwent 1 MR scan as previously described (*23*) to help analyze the PET data. Then, 13 regions of interest (ROIs) were selected from the Anatomic Automatic Labeling (AAL) template for SPM2 (*24*) in the centrum semiovale, amygdala, caudate nucleus, putamen, thalamus, cerebellum, cingulate, insula, frontal cortex, occipital cortex, parietal cortex, and temporal cortex and were applied to the PET data to generate time–activity curves using each subject's MR image to coregister the template and the PET data (*23*).

Kinetic Modeling

Volume of distribution (V_T) (*25*) values were estimated using the 1- and 2-tissue-compartment (1TC and 2TC, respectively) models (*26*). Both models included a blood volume term, with a fitted vascular fraction. In preblock studies, the occupancy of the target enzyme and the nondisplaceable volume of distribution (V_{ND}) were computed using the occupancy plot (*27*). The variability of V_T values was assessed by computing the intraclass correlation coefficient (ICC) (*28*) and the TRV, with TRV = $2 \times (V_T^{retest} - V_T^{test})/(V_T^{test} + V_T^{retest})$. The mean of TRV values (mTRV) across subjects is an index of the trend between the test and retest scans. The SD of TRV (sdTRV) is an index of the variability in V_T estimates.

Unless otherwise specified, data are presented as mean ± SD across the 15 baseline scans (first scan for each subject).

RESULTS

The radiotracer ^{11}C-AS2471907 was produced in radiochemical purity of 99.3% ± 0.5% (minimum, 98.4%, $n = 22$), with a molar activity of 190 ± 239 MBq/nmol (range, 44–1,210 MBq/nmol) at the end of synthesis.

The injected activity dose was 234 ± 114 MBq (range, 94–440 MBq) for ^{11}C-AS2471907, with an administered mass of 2.5 ± 2.6 μg (range, 0.25–9.7 μg). There were no adverse or clinically detectable pharmacologic effects in any of the 15 subjects. No significant changes in vital signs, laboratory results, or electrocardiograms were observed.

Input Functions

The parent fraction remained high through the 2-h scan: 95% ± 3% at 30 min and 85% ± 15% at 90 min after ^{11}C-AS2471907 injection (Supplemental Fig. 1; supplemental materials are available at http://jnm.snmjournals.org). Administration of the 11β-HSD1 inhibitor ASP3662 led to lower parent fractions: 81% ± 8% at 30 min and 66% ± 13% at 90 min ($n = 2$). At baseline, the SUV of ^{11}C-AS2471907 in the plasma peaked at 23 ± 5 at the end of the injection, and then decreased to 0.08 ± 0.02 at the end of the scan. The plasma clearance rate of ^{11}C-AS2471907 was 1.0 ± 0.21 L/min. The plasma concentration of ^{11}C-AS2471907 increased with preadministration of ASP3662 (Fig. 3): at the end of the scan, the plasma SUV was 1.1 ± 0.7, and the plasma clearance rate decreased to 0.21 ± 0.10 L/min ($n = 2$). Thus, blockade of the enzyme by the 11β-HSD1 inhibitor ASP3662 dramatically slowed clearance and increased tracer bioavailability. The plasma-free fraction of ^{11}C-AS2471907 was measured at 1.6% ± 0.5% at baseline and 1.4% ± 0% after ASP3662 administration. The whole-blood–to–plasma ratio was constant at 0.63 ± 0.07 for all time points and studies, indicating that the radiotracer and its metabolites do not enter blood cells.

Brain PET Images

Representative images of ^{11}C-AS2471907 in the brain are shown in Figure 4 and in Supplemental Figure 2. The rank order of regional binding, from lowest to highest peak uptake, was white matter, caudate, amygdala, insula, cingulum, frontal and temporal cortices, putamen, cerebellum, parietal cortex, thalamus, and occipital cortex. In the occipital cortex, SUV peaked at 2.7 ± 0.4 at approximately 60 min and then decreased to 2.4 ± 0.5 at 120 min. In the white matter region, the SUV_{peak} was 1.0. ± 0.2. After administration of ASP3662, ^{11}C-AS2471907 uptake was reduced dramatically in the brain, especially in regions with higher uptake at baseline: in the occipital cortex, the SUV peaked at 1.2 ± 0.2 at approximately 2 min and then decreased to 0.3 ± 0.1 at the end of the scan. Representative time–activity curves at baseline and after blockade are shown in Figure 3 and Supplemental Figure 3.

Kinetic Modeling

Representative fits of regional time–activity curves with the 1TC and 2TC models are shown in Figure 5. According to the F test, the 2TC model produced better fits ($F_{2,28} > 3.34$, $P < 0.05$) than the 1TC model in most cases (171 of 240 baseline fits, and 24 of 24 postdrug fits). At baseline, 2TC V_T values ranged from 3.7 ± 1.5 mL/cm^3 (range, 2.1–7.2 mL/cm^3) in the caudate nucleus to 14.5 ± 5.3 mL/cm^3 (range, 7.8–28 mL/cm^3) in the occipital cortex (Table 1). There was large variability in V_T values across subjects. The coefficient of variation across subjects ranged from 35% in the centrum semiovale (white matter region) to 52% in the cerebellum. The relative SE on V_T estimates was typically lower than the coefficient of variation: for the 2TC, the median relative SE ranged from 3% in the frontal cortex to 34% in the amygdala. The entry rate constant (K_1) was low: the median 2TC K_1 value ranged from 0.022 mL/min/cm^3 in the centrum semiovale to 0.070 mL/min/cm^3 in the thalamus. Though the 2TC model produced better fits in most cases, the V_T values obtained with the 1TC and 2TC models were highly correlated ($r^2 = 0.984$), with a slope close to one (0.977) and an intercept close to zero (−0.545). A Bland–Altman plot comparing 2TC and 1TC V_T values is shown in Figure 6. The high correlation between 2TC and 1TC V_T values may be in part explained by the fact that the fit in the 1TC model was poor

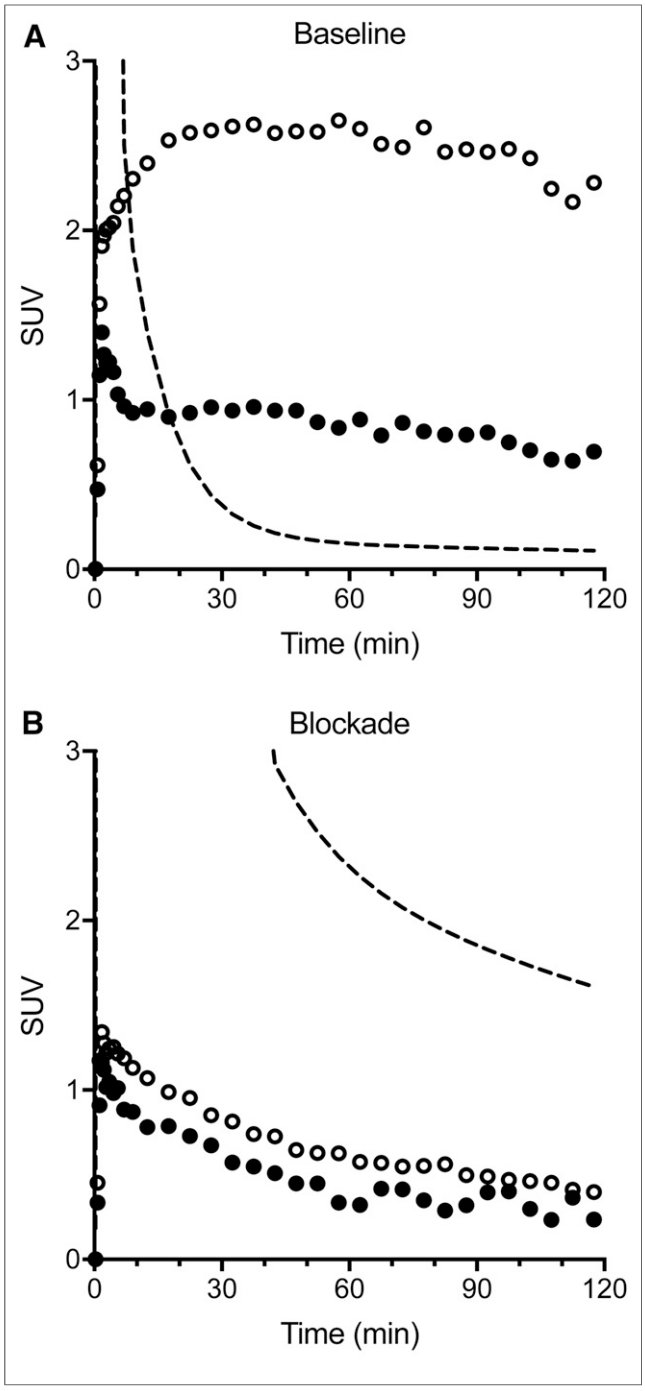

FIGURE 3. Regional time–activity curves at baseline (A) and after ASP3662 administration (B) in occipital cortex (○) and caudate (•). Dashed lines represent metabolite-corrected input function.

only in the early frame data, and became better in the later data (Fig. 5).

After administration of ASP3662, regional V_T values were drastically reduced, and ranged from 0.16 ± 0.01 mL/cm^3 in the amygdala to 0.23 ± 0.07 mL/cm^3 in the occipital cortex (Supplemental Table 1). Occupancy plots for the 2 blockade scans with ASP3662 are shown in Figure 7. The occupancy was greater than 99% in both scans, and the V_{ND} was estimated at 0.16 ± 0.04 mL/cm^3. Thus, virtually all tracer uptake in the baseline scans is specifically bound. Based on this V_{ND} estimate and the mean baseline 2TC V_T estimates, regional binding potential of ^{11}C-AS2471907 was calculated and ranged from 22 in the caudate to 90 in the occipital cortex. However, given the very low V_{ND}, it is likely that regional binding potential estimates may not be that reliable.

Test–retest summary statistics are presented in Table 2, and individual scan V_T values are shown in Supplemental Table 2. During the retest scan, ^{11}C-AS2471907 V_T values tended to be higher than those from the test scan: the average TRV value (mTRV) was positive in most regions and models. Without correction for multiple comparisons, the difference between V_T values was significant in a few regions (paired Student t test, $P < 0.05$): the cingulum; insula; and frontal, occipital, and temporal cortices (for the 2TC model). With the 2TC model, sdTRV was less than 10% in most cortical ROIs (14% in the parietal cortex) and ranged from 14% (cerebellum) to 51% (amygdala) in other ROIs. ICC values ranged from 0.55 in the centrum semiovale to 0.98 in the cerebellum, indicating that the large intersubject variability in V_T was not caused by measurement error. Comparing methods, the 2TC model produced the lowest median (across all ROIs) mTRV and sdTRV values, indicating that the simpler model did not produce less variable V_T estimates.

The effect of scan duration is presented in Supplemental Table 3. If the scan duration is reduced to 90 min, the mean bias on 2TC V_T values is on the order of 8% (median value across all ROIs), but up to 31% in small ROIs; the bias SD is on the order of 8% (median value across all ROIs), but up to 58% in the smallest ROIs. Test–retest variability (sdTRV) is also increased by 10 percentage points (median value across all ROIs) when only 90 min of data are used.

DISCUSSION

In this study, we evaluated the novel radiotracer ^{11}C-AS2471907 to quantify the distribution of the 11β-HSD1 enzyme in the brain of healthy human subjects.

The parent fraction of ^{11}C-AS2471907 in plasma remained relatively high through the scans, although clearance of ^{11}C-AS2471907

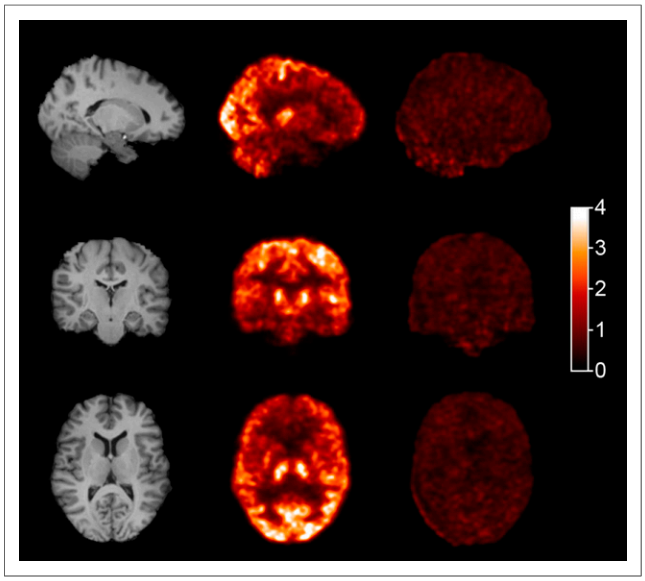

FIGURE 4. MR (left) and baseline (center) and postdrug (right) PET SUV images. Averaged from 40 to 60 min.

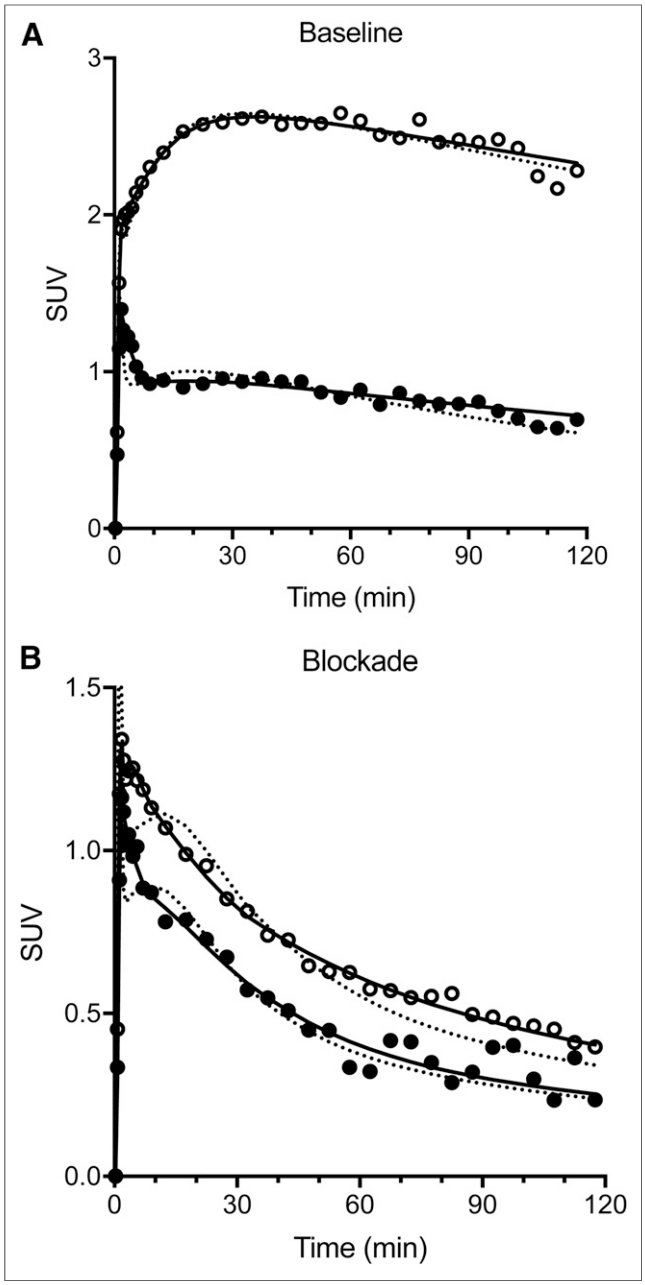

FIGURE 5. Regional time–activity curves and fitted curves at baseline (A) and after ASP3662 administration (B) in occipital cortex (○) and caudate (•). Solid lines represent 2TC model fits, and dotted lines represent 1TC model fits.

from the plasma was fast. After blockade of 11β-HSD1, plasma concentration of ^{11}C-AS2471907 increased, and the parent fraction decreased, as also seen with tracers for other targets such as serotonin transporters with a large number of binding sites in the periphery (*29*). At baseline, uptake in the brain, as measured by SUVs, ranged from 1 to 2.5, which is sufficient for imaging studies. ^{11}C-AS2471907 V_T values were well correlated with messenger RNA scores for the 11β-HSD1 gene in the Allen human brain atlas (probes 1027298 and 1027299) in the cortex ($r > 0.92$, $n = 6$, $P < 0.01$), and in all ROIs excluding the white matter ROI (centrum semiovale) ($r > 0.81$, $n = 11$, $P < 0.002$). The white matter has the highest 11β-HSD1 messenger RNA expression in the Allen atlas, which does not match the present results.

Kinetic modeling indicated that the 2TC provided better fits than the 1TC model. Moreover, the test–retest study indicated that the V_T estimates tended to be less variable with the 2TC than with the 1TC model. On the basis of these observations, the 2TC model is the recommended method for quantification of ^{11}C-AS2471907 V_T values. Because of the low uptake rate constant ($K_1 < 0.1$ mL/min/cm^3), it is also recommended to include a blood volume correction term in the model and to estimate the vascular fraction for each ROI. The low K_1 values may be due in part to the low plasma-free fraction for this tracer (~1.5%). A reference tissue model is not appropriate for this radiotracer, and likely not appropriate for any tracer targeting 11β-HSD1 due to the ubiquitous distribution of 11β-HSD1 in the brain.

Since the baseline time–activity curves were relatively flat (Fig. 3A), near-equilibrium conditions might be reached. Therefore, to evaluate whether kinetic modeling could be avoided, the tissue–to–metabolite-corrected plasma ratio (SUVR) was computed (at 60–90 min) and compared with V_T. SUVR tended to be larger than V_T in all ROIs: for example, it was 67% ± 48% higher in the occipital cortex. Moreover, the TRV of SUVR also tended to be higher than that of V_T: for example, sdTRV was 5% for V_T and 16% for SUVR in the occipital cortex. Overestimation of V_T by SUVR is expected unless washout from tissue is much faster than that from plasma (*30*), and SUVR is additionally sensitive to the variability of these 2 parameters.

Blocking studies indicated that ^{11}C-AS2471907 has specific binding in all investigated ROIs and thus that there is no reference region for this target. Moreover, ^{11}C-AS2471907 V_{ND} was very low compared with baseline V_T values, indicating that most of the tracer uptake in the brain is due to specific binding.

There was a large range of ^{11}C-AS2471907 V_T values across subjects. This difference between subjects was confirmed during the retest scans as indicated by the high ICC values for V_T estimates. The test–retest studies also indicated that V_T values from the retest scans tended to be higher than those from the test scans

TABLE 1
Regional V_T (mL/cm^3) for ^{11}C-AS2471907 in Baseline Scans

ROI	2TC	1TC
Caudate nucleus	3.7 ± 1.5	3.1 ± 1.5
Amygdala	4.3 ± 1.9	3.7 ± 1.9
Centrum semiovale	4.6 ± 1.6	3.6 ± 1.2
Cingulum	6.7 ± 2.6	5.9 ± 2.4
Insula	6.8 ± 2.8	5.9 ± 2.5
Frontal cortex	8.9 ± 3.6	8.1 ± 3.4
Putamen	9.3 ± 3.7	8.7 ± 3.8
Temporal cortex	9.4 ± 4.0	8.6 ± 3.8
Parietal cortex	11.0 ± 4.3	10.3 ± 4.2
Cerebellum	11.4 ± 5.9	10.7 ± 5.8
Thalamus	11.9 ± 5.0	11.5 ± 5.0
Occipital cortex	14.5 ± 5.3	13.5 ± 5.1

$n = 15$.

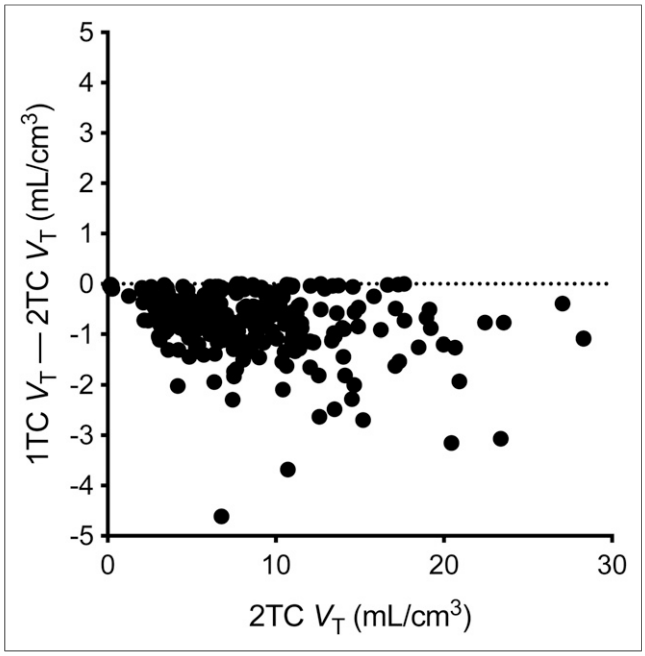

FIGURE 6. Bland–Altman plot of V_T values from 2TC and 1TC models.

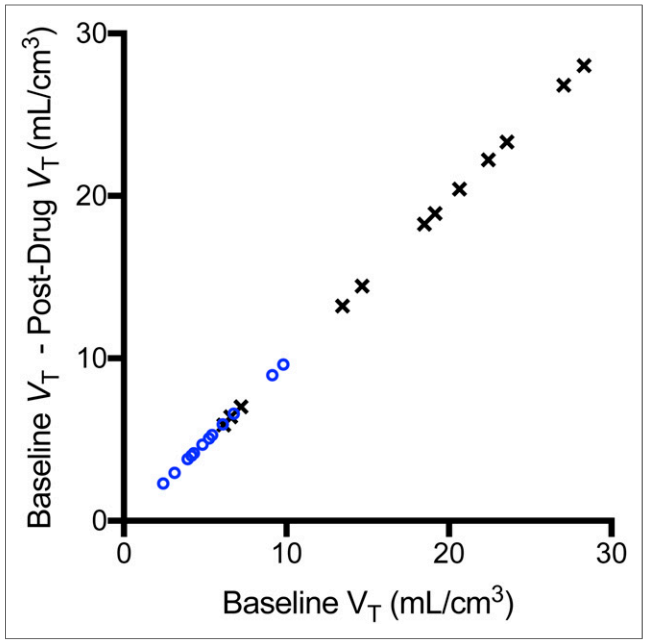

FIGURE 7. Occupancy plots for the 2 blockade studies. Occupancy was estimated to be >99% for both studies, and V_{ND} was estimated to be 0.19 ± 0.016 mL/cm^3 in first subject (black cross symbols) and 0.13 ± 0.011 mL/cm^3 in second subject (blue circles).

done earlier on the same day. This trend apparently needs verification in future studies. Nonetheless, on the basis of the current data, care should be taken in the planning of these future studies to account for this possibility. These changes in V_T values could be diurnal or habituation of the subjects to the PET procedures. Diurnal changes in cortisol levels in the periphery are well documented (*31*), however, it is not yet known if such changes occur for 11β-HSD1 in the brain. The TRV was low in large cortical ROIs (<10%) but higher in smaller ROIs. This is in part due to the low injected activity dose in these studies (234 MBq on average), leading to noisier images and data. AS2471907 is amenable to radiolabeling with ^{18}F, which is expected to improve image quality and quantification.

The recommended scan duration based on the present data is 120 min, due to increased variability of V_T estimates with shorter scans. In the future, shorter scan length may be possible if injected activity doses can be increased, or if the fluorinated version of this tracer is used.

As the first 11β-HSD1 PET radiotracer for human use, ^{11}C-AS2471907 should be useful for measuring target occupancy by 11β-HSD1 inhibitors in the brain. Second, this radiotracer can be used to compare brain occupancy by 11β-HSD1 inhibitors with functional activity of 11β-HSD1 in the brain (cerebral spinal fluid measurements) or periphery to explore single-dose or multiple-dose exposure relationships and inform optimal dose selection for clinical trials. Third, quantification of 11β-HSD1 with ^{11}C-AS2471907 would allow the investigation of whether stress-related or other diseases alter 11β-HSD1 protein expression in the brain.

CONCLUSION

To our knowledge, this is the first report of a PET radiotracer to image and quantify the enzyme 11β-HSD1 in humans. ^{11}C-AS2471907 has reasonable brain uptake and high specific binding signals in the human brain. Imaging data are modeled well with the 2TC model, and model-derived regional V_T values display fairly good within-subject test–retest reproducibility. Nonetheless, between-subject variations in regional V_T values are large, which may be due to physiologic differences among the subjects. ^{11}C-AS2471907 appears to be an appropriate radiotracer to image and quantify 11β-HSD1 in the human brain and can be used to assess enzyme occupancy of 11β-HSD1 inhibitors. However, accurate quantification of 11β-HSD1 under disease conditions may require the development of a radiotracer with better imaging characteristics.

TABLE 2
TRV of ^{11}C-AS2471907 V_T

	2TC		1TC	
ROI	TRV	ICC	TRV	ICC
Caudate nucleus	12% ± 22%	0.746	15% ± 8%	0.937
Amygdala	−7% ± 51%	0.691	1% ± 42%	0.800
Centrum semiovale	11% ± 28%	0.546	16% ± 20%	0.799
Cingulum	17% ± 8%	0.853	17% ± 14%	0.868
Insula	14% ± 9%	0.883	11% ± 18%	0.900
Frontal cortex	10% ± 7%	0.963	11% ± 14%	0.927
Putamen	10% ± 14%	0.919	11% ± 17%	0.908
Temporal cortex	14% ± 8%	0.928	13% ± 12%	0.934
Parietal cortex	13% ± 13%	0.821	13% ± 11%	0.897
Cerebellum	9% ± 14%	0.977	10% ± 15%	0.979
Thalamus	12% ± 20%	0.614	12% ± 11%	0.831
Occipital cortex	11% ± 5%	0.940	10% ± 7%	0.962

$n = 5$.

DISCLOSURE

Mark Walzer and Gerard J. Marek are employees of Astellas; Susan Bellaire and Nancy Yuan were employees of Astellas at the time of the study. This study was funded by Astellas. No other potential conflict of interest relevant to this article was reported.

REFERENCES

1. Lakshmi V, Sakai RR, McEwen BS, Monder C. Regional distribution of 11 β-hydroxysteroid dehydrogenase in rat brain. *Endocrinology.* 1991;128:1741–1748.
2. Moisan MP, Seckl JR, Brett LP, et al. 11β-hydroxysteroid dehydrogenase messenger ribonucleic acid expression, bioactivity and immunoreactivity in rat cerebellum. *J Neuroendocrinol.* 1990;2:853–858.
3. Moisan MP, Seckl JR, Edwards CR. 11 β-hydroxysteroid dehydrogenase bioactivity and messenger RNA expression in rat forebrain: localization in hypothalamus, hippocampus, and cortex. *Endocrinology.* 1990;127:1450–1455.
4. Seckl JR, Dow RC, Low SC, Edwards CR, Fink G. The 11 β-hydroxysteroid dehydrogenase inhibitor glycyrrhetinic acid affects corticosteroid feedback regulation of hypothalamic corticotrophin-releasing peptides in rats. *J Endocrinol.* 1993;136:471–477.
5. Sandeep TC, Yau JL, MacLullich AM, et al. 11β-hydroxysteroid dehydrogenase inhibition improves cognitive function in healthy elderly men and type 2 diabetics. *Proc Natl Acad Sci USA.* 2004;101:6734–6739.
6. Harris HJ, Kotelevtsev Y, Mullins JJ, Seckl JR, Holmes MC. Intracellular regeneration of glucocorticoids by 11β-hydroxysteroid dehydrogenase (11β-HSD)-1 plays a key role in regulation of the hypothalamic-pituitary-adrenal axis: analysis of 11β-HSD-1-deficient mice. *Endocrinology.* 2001;142:114–120.
7. Swaab DF, Bao AM, Lucassen PJ. The stress system in the human brain in depression and neurodegeneration. *Ageing Res Rev.* 2005;4:141–194.
8. Sinha R. Chronic stress, drug use, and vulnerability to addiction. *Ann N Y Acad Sci.* 2008;1141:105–130.
9. Stephens MA, Wand G. Stress and the HPA axis: role of glucocorticoids in alcohol dependence. *Alcohol Res.* 2012;34:468–483.
10. Meaney MJ, O'Donnell D, Rowe W, et al. Individual differences in hypothalamic-pituitary-adrenal activity in later life and hippocampal aging. *Exp Gerontol.* 1995;30:229–251.
11. Holmes MC, Carter RN, Noble J, et al. 11β-hydroxysteroid dehydrogenase type 1 expression is increased in the aged mouse hippocampus and parietal cortex and causes memory impairments. *J Neurosci.* 2010;30:6916–6920.
12. Holmes MC, Seckl JR. The role of 11β-hydroxysteroid dehydrogenases in the brain. *Mol Cell Endocrinol.* 2006;248:9–14.
13. Mohler EG, Browman KE, Roderwald VA, et al. Acute inhibition of 11β-hydroxysteroid dehydrogenase type-1 improves memory in rodent models of cognition. *J Neurosci.* 2011;31:5406–5413.
14. Yau JL, McNair KM, Noble J, et al. Enhanced hippocampal long-term potentiation and spatial learning in aged 11β-hydroxysteroid dehydrogenase type 1 knock-out mice. *J Neurosci.* 2007;27:10487–10496.
15. Yau JL, Noble J, Kenyon CJ, et al. Lack of tissue glucocorticoid reactivation in 11β-hydroxysteroid dehydrogenase type 1 knockout mice ameliorates age-related learning impairments. *Proc Natl Acad Sci USA.* 2001;98:4716–4721.
16. Sooy K, Webster SP, Noble J, et al. Partial deficiency or short-term inhibition of 11β-hydroxysteroid dehydrogenase type 1 improves cognitive function in aging mice. *J Neurosci.* 2010;30:13867–13872.
17. Sooy K, Noble J, McBride A, et al. Cognitive and disease-modifying effects of 11β-hydroxysteroid dehydrogenase type 1 inhibition in male Tg2576 mice, a model of Alzheimer's disease. *Endocrinology.* 2015;156:4592–4603.
18. Yarchoan M, Arnold SE. Repurposing diabetes drugs for brain insulin resistance in Alzheimer disease. *Diabetes.* 2014;63:2253–2261.
19. Li W, Joshi A, Zeng Z, et al. Radiosynthesis and evaluation of an 11-β hydroxysteroid dehydrogenase-1 (11β-HSD1) PET ligand in rhesus monkey. *J Label Compd Radiopharm.* 2011;54:S293.
20. Kiso T, Sekizawa T, Uchino H, Tsukamoto M, Kakimoto S. Analgesic effect of ASP3662, a novel 11β-HSD1 inhibitor, in rat models of neuropathic and dysfunctional pain. *Br J Pharmacol.* 2018;175:3784–3796.
21. Hannestad J, Dellagioia N, Gallezot J-D, et al. The neuroinflammation marker translocator protein is not elevated in individuals with mild-to-moderate depression: a [^{11}C]PBR28 PET study. *Brain Behav Immun.* 2013;33:131–138.
22. Lin S-F, Labaree D, Chen M-K, et al. Further evaluation of [^{11}C]MP-10 as a radiotracer for phosphodiesterase 10A: PET imaging study in rhesus monkeys and brain tissue metabolite analysis. *Synapse.* 2015;69:86–95.
23. Naganawa M, Waterhouse RN, Nabulsi NB, et al. First in human assessment of the novel PDE2A PET radiotracer ^{18}F-PF-05270430. *J Nucl Med.* 2016;57:1388–1395.
24. Tzourio-Mazoyer N, Landeau B, Papathanassiou D, et al. Automated anatomical labeling of activations in SPM using a macroscopic anatomical parcellation of the MNI MRI single-subject brain. *Neuroimage.* 2002;15:273–289.
25. Innis RB, Cunningham VJ, Delforge J, et al. Consensus nomenclature for in vivo imaging of reversibly binding radioligands. *J Cereb Blood Flow Metab.* 2007;27:1533–1539.
26. Gunn RN, Gunn SR, Cunningham VJ. Positron emission tomography compartmental models. *J Cereb Blood Flow Metab.* 2001;21:635–652.
27. Cunningham VJ, Rabiner EA, Slifstein M, Laruelle M, Gunn RN. Measuring drug occupancy in the absence of a reference region: the Lassen plot re-visited. *J Cereb Blood Flow Metab.* 2010;30:46–50.
28. Shrout PE, Fleiss JL. Intraclass correlations: uses in assessing rater reliability. *Psychol Bull.* 1979;86:420–428.
29. Huang Y, Hwang D-R, Bae S-A, et al. A new positron emission tomography imaging agent for the serotonin transporter: synthesis, pharmacological characterization, and kinetic analysis of [^{11}C]2-[2-(dimethylaminomethyl)phenylthio]-5-fluoromethylphenylamine ([^{11}C]AFM). *Nucl Med Biol.* 2004;31:543–556.
30. Carson RE. PET physiological measurements using constant infusion. *Nucl Med Biol.* 2000;27:657–660.
31. Edwards S, Evans P, Hucklebridge F, Clow A. Association between time of awakening and diurnal cortisol secretory activity. *Psychoneuroendocrinology.* 2001;26:613–622.